

# The conductivity of dense molecular gas

Mark Wardle<sup>1</sup> & Cindy Ng<sup>2</sup>

<sup>1</sup>*Special Research Centre for Theoretical Astrophysics, University of Sydney, NSW 2006, Australia*

<sup>2</sup>*Department of Physics, University of Tasmania, Hobart, TAS 7001, Australia*

MNRAS accepted 1998 October 21

## ABSTRACT

We evaluate the conductivity tensor for molecular gas at densities ranging from  $10^4$  to  $10^{15}$   $\text{cm}^{-3}$  for a variety of grain models. The Hall contribution to the conductivity has generally been neglected in treatments of the dynamics of molecular gas. We find that it is not important if only  $0.1 \mu\text{m}$  grains are considered, but for a Mathis-Rumpl-Nordsieck grain-size distribution (with or without PAHs) it becomes important for densities between  $10^7$  and  $10^{11}$   $\text{cm}^{-3}$ . If PAHs are included, this range is reduced to  $10^9$ – $10^{10}$   $\text{cm}^{-3}$ .

The consequences for the magnetic field evolution and dynamics of dense molecular gas are profound. To illustrate this, we consider the propagation of Alfvén waves under these conditions. A linear analysis yields a dispersion relation valid for frequencies below the neutral collision frequencies of the charged species. The dispersion relation shows that there is a pair of circularly polarised modes with distinct propagation speeds and damping rates. We note that the gravitational collapse of dense cloud cores may be substantially modified by the Hall term.

**Key words:** magnetohydrodynamics – Alfvén waves – dust grains – molecular clouds.

## 1 INTRODUCTION

The breakdown of flux-freezing in molecular clouds has generally been treated using the concept of “ambipolar diffusion” (e.g. Spitzer 1978). In this approximation the magnetic field is regarded as being frozen into the *ionised* component of the fluid, which drifts as a whole with respect to the neutrals. During ambipolar diffusion, the magnetic stresses operating on the ionised plasma are transmitted to the dominant neutral component via collisions. The resulting dissipation damps MHD waves (Kulsrud & Pearce 1969) and is particularly important in shock waves where it provides the heating within the shock front (Draine 1980). Ambipolar diffusion allows the trickling of neutrals through the ions and magnetic field towards the centre of a dense core until the core becomes gravitationally unstable and collapses (see e.g. Mouschovias 1987; Fiedler & Mouschovias 1993).

The ambipolar-diffusion approximation is valid when the magnetic force on each charged particle dominates the drag force arising through collisions with the neutrals (i.e. the product of the gyrofrequency and the time scale for momentum-exchange with the neutrals is much greater than unity). This is generally an excellent approximation for ions and electrons in molecular clouds, except for densities and magnetic field strengths appropriate for protostellar disks (Norman & Heyvaerts 1985; Wardle & Königl 1993).

Charged grains, however, are partially decoupled from the magnetic field by neutral collisions because of their large

geometrical cross-section. This effect has generally been treated by including a separate equation of motion for the grains so that their drift speed through the neutrals can be calculated (see e.g. Draine 1980). The current density then has a component out of the plane containing the magnetic field and the electric field in the rest frame of the neutral fluid. This component, the Hall current, has generally been suppressed in calculations of gravitational condensation via ambipolar diffusion (Ciolek & Mouschovias 1993), and in shock modelling (e.g. Draine, Roberge & Dalgarno 1983; Wardle & Draine 1987; Kaufman & Neufeld 1996). This is a poor approximation when the grain drag is important (typically at densities in excess of  $10^6$   $\text{cm}^{-3}$ ). In the case of shock waves, when this component is retained the shock structure is significantly thinner (Pilipp, Hartquist & Havnes 1990) and is qualitatively different, exhibiting a twist back and forth around the preshock normal (Wardle 1998).

Early studies assumed that grains were of a single characteristic size (typically  $0.1 \mu\text{m}$ ). It has since been recognised that the MRN grain-size distribution (Mathis, Rumpl & Nordsieck 1977) and the presence of polycyclic aromatic hydrocarbons (PAHs) (Leger & Puget 1984) imply that grains play a more important role in coupling the magnetic field to the neutral gas (Nishi, Nakano & Umeyayashi 1991), grains and PAHs being the dominant charged species above  $10^7$   $\text{cm}^{-3}$ .

Here we examine the conductivity of molecular gas at densities relevant to cloud cores, and at higher densities oc-

arXiv:astro-ph/9810468v1 28 Oct 1998

curing during the formation of a protostar and its associated disk. We formulate MHD in §2 in terms of a conductivity tensor appropriate for a weakly-ionised gas (Cowling 1957; Norman & Heyvaerts 1985; Nakano & Umebayashi 1986) and stress that the *vector* evolution of the magnetic field depends on the relative magnitudes of the different components. We evaluate the conductivity for single-size, MRN, and MRN-plus-PAH grain models in §3, with charged particle abundances from Umebayashi & Nakano (1990) and Nishi et al (1991). We find that the Hall term is not particularly important in the single-size grain model, but in the other models becomes important for densities between  $10^7$  and  $10^{11}$   $\text{cm}^{-3}$ . The dynamical behaviour of molecular gas at higher densities is therefore profoundly different from the ambipolar diffusion case. By way of illustration we consider the propagation of Alfvén waves in §4. The implications of our results are further discussed in §5, and our conclusions are summarised in §6.

## 2 FORMULATION

### 2.1 MHD in weakly-ionised media

Our definition of “weakly-ionised” is that the abundances of charged species are so low that their inertia and thermal pressure is negligible, and that the changes in the neutral gas resulting from ionisation and recombination are so small that they may also be neglected.

In this limit, the fluid equations may be written

$$\frac{\partial \rho}{\partial t} + \nabla \cdot (\rho \mathbf{v}) = 0, \quad (1)$$

$$\rho \frac{\partial \mathbf{v}}{\partial t} + \rho(\mathbf{v} \cdot \nabla) \mathbf{v} + c_s^2 \nabla \rho = \frac{\mathbf{J} \times \mathbf{B}}{c}, \quad (2)$$

where  $c_s^2$ , the isothermal sound speed, is assumed to be constant,

$$\mathbf{J} = \frac{c}{4\pi} \nabla \times \mathbf{B}, \quad (3)$$

$$\frac{\partial \mathbf{B}}{\partial t} = \nabla \times (\mathbf{v} \times \mathbf{B}) - c \nabla \times \mathbf{E}', \quad (4)$$

and

$$\nabla \cdot \mathbf{B} = 0. \quad (5)$$

Here

$$\mathbf{E}' = \mathbf{E} + \mathbf{v} \times \mathbf{B}/c \quad (6)$$

is the electric field in the frame comoving with the fluid, which is related to the current density by the conductivity tensor  $\boldsymbol{\sigma}$ :

$$\mathbf{J} = \boldsymbol{\sigma} \cdot \mathbf{E}'. \quad (7)$$

We shall consider an explicit expression for  $\boldsymbol{\sigma}$  in the next subsection. For now, we merely note that all of the information concerning the charged species is hidden in  $\boldsymbol{\sigma}$ , and that we are implicitly assuming a prescription for determining the abundances of the charged species so that the conductivity can be calculated.

At this point we emphasise the role that the conductivity plays in determining the evolution of the magnetic field through the induction equation (4), which on substituting for  $\mathbf{E}'$  becomes:

$$\frac{\partial \mathbf{B}}{\partial t} = \nabla \times (\mathbf{v} \times \mathbf{B}) - \frac{c^2}{4\pi} \nabla \times [\boldsymbol{\sigma}^{-1} \cdot (\nabla \times \mathbf{B})]. \quad (8)$$

The second term becomes important if the current associated with the gradient in the magnetic field is so large that  $|\mathbf{E}'|$  is comparable to or greater than  $|\mathbf{v} \times \mathbf{B}|/c$ . The magnitude of the conductivity determines a characteristic length scale (or time scale) below which the field cannot be regarded as frozen-in (see e.g. Parker 1979). It is not, however, the magnitude on which we wish to focus but rather the *tensor* nature of the conductivity, which affects the *direction* of  $\partial \mathbf{B}/\partial t$ . That is, the vector evolution of  $\mathbf{B}$  from an initial configuration depends on the relative magnitude of the components of  $\boldsymbol{\sigma}$ .

### 2.2 The conductivity tensor

We characterise the various charged species in the neutral fluid by particle mass  $m_j$  and charge  $Z_j e$ , number density  $n_j$ , and drift velocity through the neutral gas  $\mathbf{v}_j$ , where the subscript  $j$  denotes different species. Note that we have already implicitly assumed charge neutrality, i.e.

$$\sum_j n_j Z_j = 0. \quad (9)$$

Assuming that the fluid evolves on a time scale that is long compared to the collision time scale of any type of charged particle with the neutrals, each charged particle drifts through the neutrals at a rate and direction determined by the instantaneous Lorentz force on the particle:

$$Z_j e (\mathbf{E}' + \frac{\mathbf{v}_j}{c} \times \mathbf{B}) - \gamma_j m_j \mathbf{v}_j = 0, \quad (10)$$

where the third term represents the drag force contributed by collisions with the neutrals, and

$$\gamma_j = \frac{\langle \sigma v \rangle_j}{m_j + m} \quad (11)$$

where  $\langle \sigma v \rangle_j$  is the rate coefficient for momentum transfer by collisions with the neutrals and  $m$  is the mean neutral particle mass. The Hall parameter for species  $j$ ,

$$\beta_j = \frac{Z_j e B}{m_j c} \frac{1}{\gamma_j \rho}, \quad (12)$$

determines the relative importance of the Lorentz and drag forces in balancing the electric force.

Eq (10) can be inverted for  $\mathbf{v}_j$ , which can then be used to form an expression for  $\mathbf{J} = e \sum_j n_j Z_j \mathbf{v}_j$ :

$$\mathbf{J} = \sigma_{\parallel} \mathbf{E}'_{\parallel} + \sigma_1 \hat{\mathbf{B}} \times \mathbf{E}'_{\perp} + \sigma_2 \mathbf{E}'_{\perp} \quad (13)$$

where  $\mathbf{E}'_{\parallel}$  and  $\mathbf{E}'_{\perp}$  are the decomposition of  $\mathbf{E}'$  into vectors parallel and perpendicular to  $\mathbf{B}$  respectively. The components of  $\boldsymbol{\sigma}$  are the conductivity parallel to the magnetic field,

$$\sigma_{\parallel} = \frac{ec}{B} \sum_j n_j Z_j \beta_j, \quad (14)$$

the Hall conductivity,

$$\sigma_1 = \frac{ec}{B} \sum_j \frac{n_j Z_j}{1 + \beta_j^2}, \quad (15)$$

and the Pedersen conductivity

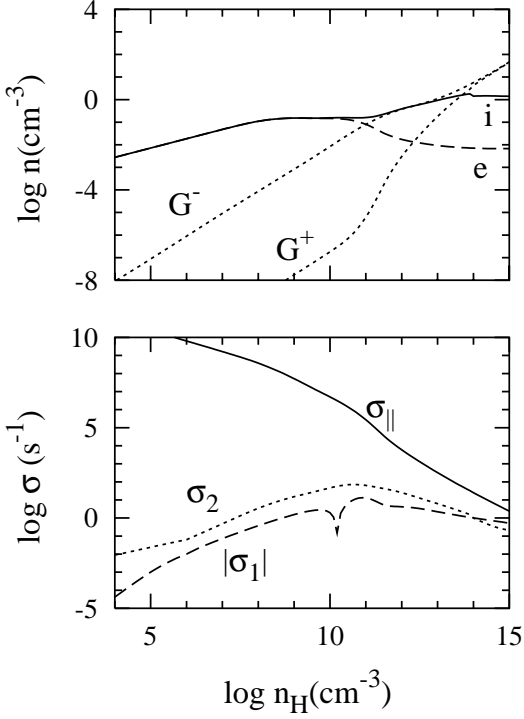


**Figure 1.** *Upper panel:* the abundances of charged species when grains have size  $0.1 \mu\text{m}$ . The curves labelled  $i$ ,  $e$ ,  $G^+$  and  $G^-$  refer to ions, electrons and positively and negatively charged grains respectively (adapted from Umebayashi & Nakano 1990). *Lower panel:* the field-parallel ( $\sigma_{\parallel}$ ), Hall ( $\sigma_1$ ) and Pedersen ( $\sigma_2$ ) components of the conductivity tensor. The ambipolar-diffusion approximation is valid for  $|\sigma_1| \ll \sigma_2 \ll \sigma_{\parallel}$ . The spike in the curve for  $|\sigma_1|$  at  $n_{\text{H}} \approx 10^{10} \text{ cm}^{-3}$  occurs because  $\sigma_1$  is negative at lower densities and positive at higher densities.

$$\sigma_2 = \frac{ec}{B} \sum_j \frac{n_j Z_j \beta_j}{1 + \beta_j^2} \quad (16)$$

(Cowling 1957; Norman & Heyvaerts 1985; Nakano & Umebayashi 1986). We shall find it useful to refer to the total conductivity perpendicular to the field,

$$\sigma_{\perp} = \sqrt{\sigma_1^2 + \sigma_2^2}. \quad (17)$$

Three conductivity regimes are delineated by the magnitude of the typical Hall parameter,  $\beta$ , of the charged species:

- (i)  $|\beta| \gg 1$ , which implies that  $\sigma_{\parallel} \gg \sigma_2 \gg |\sigma_1|$  and gives rise to the ambipolar diffusion regime;
- (ii)  $|\beta| \ll 1$ , which yields  $\sigma_{\parallel} \approx \sigma_2 \gg |\sigma_1|$ , implying that the conductivity is scalar ( $\mathbf{J} \approx \sigma_{\parallel} \mathbf{E}'$ ) – the resistive regime; and
- (iii)  $|\beta| \approx 1$ , the Hall regime.

The latter has been largely neglected, but we shall see that the grain-size distribution implies that it is relevant over a broad range of conditions in dense molecular gas.

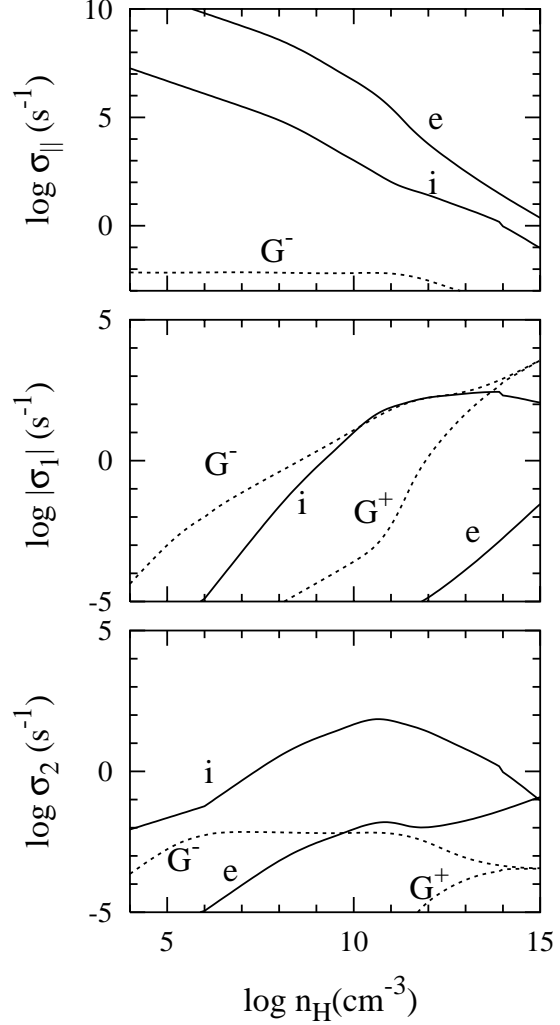


**Figure 2.** The contributions made by different species to the components of the conductivity tensor plotted in Fig. 1. Note that the positive and negative species contribute positive and negative terms to  $\sigma_1$  respectively, but that all species contribute positively to  $\sigma_{\parallel}$  and  $\sigma_2$ .

### 3 CONDUCTIVITY IN DENSE MOLECULAR GAS

The conductivity tensor depends on the abundances of charged species, which in turn depend on the choice of grain model as recombination generally occurs on the surface of grains (Nishi et al 1991). We adopt three grain models:

- (i) Single-size grains, characterised by a grain radius  $0.1 \mu\text{m}$  and a total grain mass that is one percent of the total mass in hydrogen.
- (ii) An MRN model with a power-law distribution of grain sizes between 50 and 2500  $\text{\AA}$ :

$$\frac{dn}{da} = An_{\text{H}} a^{-3.5}, \quad (18)$$

where  $n(a)$  is the number density of grains with radii smaller than  $a$ , and  $A = 1.5 \times 10^{-25} \text{ cm}^{-2.5}$  (Draine & Lee 1984).

- (iii) An MRN model with an additional component of very small grains with  $a \sim 3 \text{ \AA}$ , representing PAHs with an abundance  $n_g/n_{\text{H}} = 2 \times 10^{-7}$ .

To evaluate the conductivity, we obtain the abundances of charged species from Fig. 2 of Umebayashi & Nakano (1990) and Figs 1 and 4 of Nishi et al (1991). The species we include are molecular and metal ions  $i$ , electrons  $e$ , MRN grains ( $G^+$ ,  $G^-$ ) and PAHs ( $g^+$ ,  $g^-$ ). The rate coefficients for momentum transfer by elastic scattering of species  $j$  with neutrals,  $\langle \sigma v \rangle_j$  are given by

$$\langle \sigma v \rangle_i = \langle \sigma v \rangle_g = 1.6 \times 10^{-9} \text{ cm}^3 \text{ s}^{-1}, \quad (19)$$

$$\langle \sigma v \rangle_e = 1 \times 10^{-15} \text{ cm}^2 \left( \frac{128kT_e}{9\pi m_e} \right)^{1/2}, \quad (20)$$

and

$$\langle \sigma v \rangle_G = \pi a^2 \left( \frac{128kT}{9\pi m} \right)^{1/2}, \quad (21)$$

where  $T$  and  $T_e$  are the neutral and electron temperatures respectively. The rate coefficient for the PAHs has been set equal to that for the ions as the induced-polarisation cross-section dominates the geometric cross-section for charged particles with sizes below  $10 \text{ \AA}$ . The expressions for  $\langle \sigma v \rangle_G$  and  $\langle \sigma v \rangle_e$  are valid as long as the grain and electron drift speeds are less than the sound speeds in the neutrals and electrons respectively.

To calculate the conductivities, we adopt  $T = T_e = 30 \text{ K}$ , a cosmic-ray ionisation rate per hydrogen nucleus  $\zeta = 10^{-17} \text{ s}^{-1} \text{ H}^{-1}$ ,  $m = 2.33m_p$  corresponding to a helium abundance of 0.1 by number, and a magnetic field that follows the standard  $n_H^{1/2}$  scaling for densities below  $10^6 \text{ cm}^{-3}$  (Myers & Goodman 1988) with a weaker dependence at higher densities:

$$\left( \frac{B}{\text{mG}} \right) = \begin{cases} (n_H/10^6 \text{ cm}^{-3})^{1/2} & \text{if } n_H < 10^6 \text{ cm}^{-3}, \\ (n_H/10^6 \text{ cm}^{-3})^{1/4} & \text{otherwise.} \end{cases} \quad (22)$$

When integrating over the MRN size distribution we have assumed that the ratio of charged to neutral grains is independent of grain radius.

The upper panel of Figure 1 shows the charged particle densities for the single-size grain model. Ions and electrons are the dominant charged species for  $n_H \lesssim 10^{10} \text{ cm}^{-3}$ , negatively-charged grains replace the electrons for  $n_H \gtrsim 10^{11} \text{ cm}^{-3}$ , and above  $10^{14} \text{ cm}^{-3}$  ions are dominated by positively charged grains. The three components of the conductivity tensor are plotted in the lower panel.  $\sigma_{\parallel}$  dominates the other two components until  $n_H \gtrsim 10^{15} \text{ cm}^{-3}$ . Below about  $10^{10} \text{ cm}^{-3}$ , the Hall term  $\sigma_1$  is negative and is typically an order of magnitude below the Pedersen term,  $\sigma_2$ .  $\sigma_1$  changes sign at roughly  $10^{10} \text{ cm}^{-3}$ . Above this density,  $|\sigma_1|$  approaches  $\sigma_2$  and the ambipolar diffusion approximation breaks down for  $n_H \gtrsim 10^{13} \text{ cm}^{-3}$ .

The contributions of different charged species to the components of  $\sigma$  are plotted in Figure 2. It should be noted that each species contributes positively to both  $\sigma_{\parallel}$  and  $\sigma_2$ , but that the contribution to  $\sigma_1$  carries the sign of  $Z_j$ . The conductivity parallel to the magnetic field is dominated by the electrons, even when much less abundant than the other charged species, because of their low rate coefficient for neutral scattering. As one might expect, the grain contributions are negligible because of their large collision cross-section with the neutrals. Negatively charged grains dominate the Hall term below  $10^{10} \text{ cm}^{-3}$  at which point the ion Hall parameter has dropped to order unity, the ion contribution

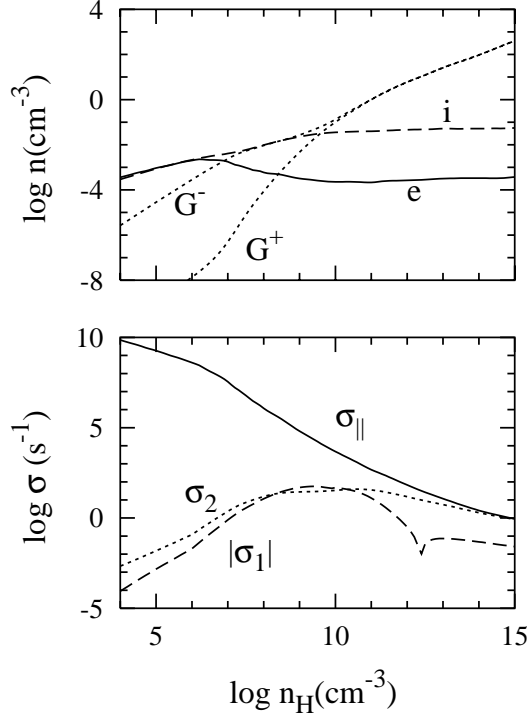


**Figure 3.** As for Fig. 1, but for an MRN grain-size distribution.

takes over and  $\sigma_1$  becomes positive. At the highest densities, positive grains are also important. The Pedersen conductivity  $\sigma_2$  is determined by the ions, except at the very highest densities when electrons start to contribute.

The abundances and conductivity for the MRN model are plotted in Figure 3. There are many more grains than in the single-size grain model, and grains therefore play a significant role in the ionisation balance at lower densities (Nishi et al 1991). Negatively charged grains dominate the electrons for  $n_H \gtrsim 10^7 \text{ cm}^{-3}$ , and positive grains dominate ions above  $10^{10} \text{ cm}^{-3}$ . The drop in electron no. density reduces  $\sigma_{\parallel}$  considerably, but  $\sigma_{\parallel}$  is still much larger than the other components for  $n_H \lesssim 10^{12} \text{ cm}^{-3}$ .  $\sigma_1$  becomes comparable to  $\sigma_2$  between  $10^7 \text{ cm}^{-3}$  and  $10^{11} \text{ cm}^{-3}$ . It drops sharply at higher densities, changing sign at  $10^{12} \text{ cm}^{-3}$ .

Fig. 4 shows which species contribute to the components of  $\sigma$ . Electrons again dominate  $\sigma_{\parallel}$ , but  $\sigma_1$  and  $\sigma_2$  are determined by the grains. Note that for  $n_H \gtrsim 10^{10} \text{ cm}^{-3}$ , the positive and negative grains contribute nearly-equal terms of opposite sign to the Hall conductivity. The slightly depressed abundance of positive grains (of order 0.1–1%) is sufficient for the net grain contribution to  $\sigma_1$  to dominate  $\sigma_2$ . Above  $10^{11} \text{ cm}^{-3}$  the asymmetry drops to the point that  $|\sigma_1|$  is a small fraction of  $\sigma_2$ , becoming dominated by the ion contribution above  $10^{12} \text{ cm}^{-3}$ .

Finally, the effects of a PAH population are shown in Figures 5 and 6. Ions and PAHs are the dominant charged species between  $10^6$ – $10^9 \text{ cm}^{-3}$ . For  $n_H \gtrsim 10^9 \text{ cm}^{-3}$  PAHs and grains of either sign are important. Despite the change to the charged particle abundances, the components of the conductivity tensor behave similarly to the MRN-only case, with  $|\sigma_1| \approx \sigma_2$  between  $10^8$  and  $10^{11} \text{ cm}^{-3}$ . Electrons con-

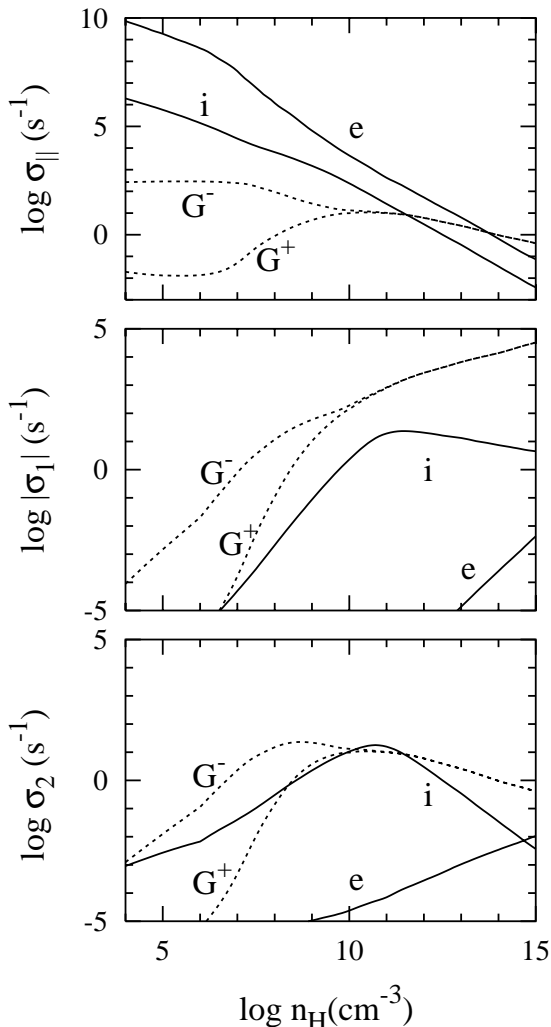


**Figure 4.** As for Fig. 2, but for an MRN grain-size distribution.

continue to dominate  $\sigma_{\parallel}$  below  $10^{10} \text{ cm}^{-3}$ , with PAHs dominating at higher densities. Grains determine  $\sigma_1$  and  $\sigma_2$ , with PAHs becoming important above  $10^{10} \text{ cm}^{-3}$ .

A broad range of magnetic field strengths are appropriate to any particular value of the gas density, so it is important to consider the effects of departures of the magnetic field from the scaling (22). Thus we show in Fig. 7 how the ratio  $|\sigma_1|/\sigma_2$  depends on both  $B$  and  $n_{\text{H}}$  for the MRN grain model. Consider first the solid contours, which refer to a gas temperature of 30 K. The innermost contour corresponds to a ratio of unity, with successive contours indicating where  $|\sigma_1|/\sigma_2 = 0.1$ , and 0.01. The gradients are weakest parallel to lines of constant  $B/n_{\text{H}}$  as the Hall parameters are constant and  $\sigma$  varies only as a result of the density-dependence of the  $n_j$ . The dashed trajectory indicates the scaling of  $B$  with  $n_{\text{H}}$  from eq. (22), thus Figure 3 shows  $\sigma$  for cuts taken along this trajectory. It is clear that  $|\sigma_1| \gtrsim \sigma_2$  over a significant region at densities characteristic of dense cores. In addition there is a region at higher densities ( $n_{\text{H}} \approx 10^{11} - 10^{13} \text{ cm}^{-3}$ ) and mG field strengths in which the ratio is greater than 0.1. The dashed curves show the effect of increasing the temperature to 300 K, which increases the electron and grain momentum-transfer rate co-

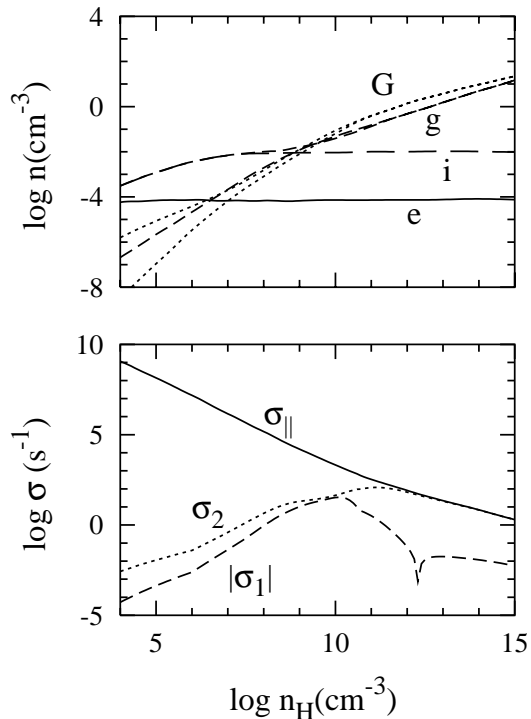


**Figure 5.** As for Fig. 1, but for an MRN grain-size distribution and PAHs

efficients and generally increases  $|\sigma_1|/\sigma_2$  (note that the effects of the increased temperature on the charged-particle abundances have not been included).

#### 4 ALFVÉN WAVES

The results of the previous section show that the Hall term is significant for molecular gas densities in the range  $10^8 - 10^{11} \text{ cm}^{-3}$ . As outlined in §2 this will have consequences for dynamical processes, particularly for the time-evolution of magnetic fields from an initial state. By way of illustration, we consider here the propagation of Alfvén waves in weakly-ionised media.

Linear wave propagation in molecular clouds has previously been studied by Kulsrud & Pearce (1969), who assumed a plasma comprised of neutrals, ions and electrons, and showed that short wavelengths are rapidly damped by ion-neutral friction. Pilipp et al (1987) examined the influence of charged grains, assumed to be all of the same size. Pilipp et al considered interactions between charged species and the coupling between the charged and neutral grain fluids that results from charging and neutralisation processes. Propagation at an oblique angle to the magnetic field has been considered by Cramer & Vladimirov (1997).

Here we present a simpler treatment using the formulation of §2, which neglects the inertia of the charged species, and thus is valid for wave frequencies  $\omega$  below the collision frequencies  $\gamma_j \rho$  of the charged species with the neutrals. This also permits us to neglect the coupling between charged and neutral grains, which generally is only important at even higher frequencies (Pilipp et al 1987).

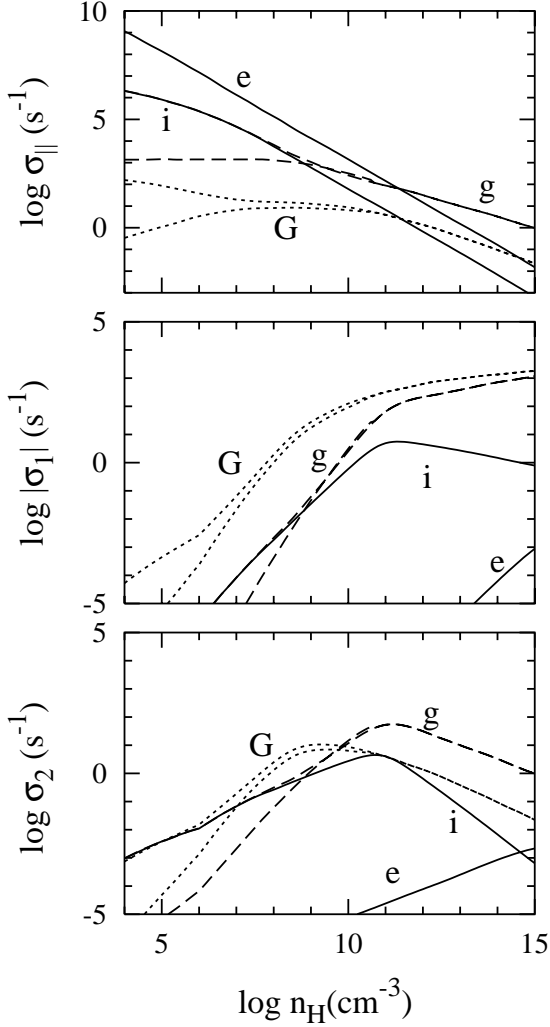


**Figure 6.** As for Fig. 2, but for an MRN grain-size distribution and PAHs.

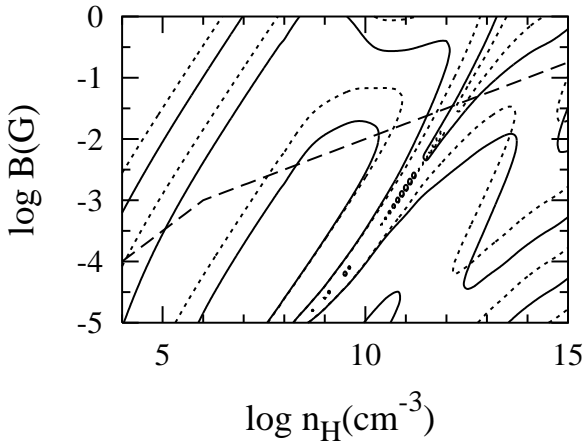


**Figure 7.** The ratio  $|\sigma_1|/\sigma_2$  for temperatures of 30 and 300 K (solid and dotted contours respectively). The contours are spaced logarithmically, with levels 1, 0.1, and 0.01. The dashed curve indicates the magnetic field scaling adopted in calculating Figs 1 – 6.

We begin by estimating the frequency  $\omega_c$  at which flux freezing breaks down, and showing that  $\omega_c \ll \gamma\rho_j$ . This guarantees that our treatment applies to the interesting regime  $\omega \sim \omega_c$ . For long-wavelength disturbances, the  $c\nabla \times \mathbf{E}'$  term in the induction equation (4) is negligible and the effects of finite conductivity are small: the dispersion relation for Alfvén waves is simply  $\omega \approx kv_A$ . At successively shorter wavelengths the  $c\nabla \times \mathbf{E}'$  term becomes increasingly important, and the wave modes are strongly modified by the finite conductivity when  $\omega \approx (\omega/v_A)^2 c^2/4\pi\sigma_\perp$ , i.e. at a critical frequency

$$\omega_c = \frac{B^2 \sigma_\perp}{\rho c^2}. \quad (23)$$

Substituting for  $\sigma_\perp$  using equations (17) and (12), and noting that the norm of a sum of vectors is less than the sum of the norms, we obtain a limit on  $\omega_c$ :

$$\omega_c < \sum_j \frac{\gamma_j \rho_j |\beta_j|}{\sqrt{1 + \beta_j^2}} < \sum_j \gamma_j \rho_j. \quad (24)$$

Strict equality is approached in the limit  $|\beta_j| \rightarrow \infty$ , i.e. when all of the charged species are tied to the magnetic field lines, in which case  $\omega_c$  is the collision frequency of the neutrals with any of the charged species. More generally,  $\omega_c$  is less than this and, as  $\rho_j \ll \rho$ , is clearly much less than  $\gamma\rho_j$  for any charged species  $j$ . The smallest  $\gamma_j\rho$  is that for the largest (i.e. 0.1  $\mu\text{m}$ ) grains. In dense clouds,  $\gamma_G\rho_G \sim \gamma_i\rho_i$ , thus  $\omega_c \sim \gamma_G\rho_G$ . As the mass in grains is of order a percent of the neutral gas, and only a fraction of the grains are charged, this implies that the dispersion relation we obtain below is valid for frequencies up to at least  $100\omega_c$ . At higher frequencies the neutral component does not play a significant dynamical role but merely provides a background drag that damps small-scale disturbances in the ionised component of the fluid.

#### 4.1 Linearisation

We linearise equations (1), (2), (3), (6), and (13) about a homogeneous undisturbed state with  $\mathbf{v} = 0$ ,  $\mathbf{J} = \mathbf{E}' = 0$ , and  $\mathbf{B} = B\mathbf{x}$ . Changes in the conductivity associated with the perturbations do not appear in the linearised equations, as  $\mathbf{E}'$  vanishes in the unperturbed state. Thus we need not make any assumptions about how the charged particle abundances respond to the perturbations – all that is needed is the conductivity tensor of the unperturbed fluid.

Considering waves propagating parallel to  $\mathbf{B}$  of the form  $\exp(i(\omega t - kx))$ , and discarding an additional quadratic factor that yields the familiar isothermal sound waves propagating parallel and antiparallel to the magnetic field, we find that  $\omega$  and  $k$  are related by the two dispersion relations

$$\omega^2 \mp k^2 v_A^2 \exp(\pm i\theta) \omega / \omega_c - k^2 v_A^2 = 0 \quad (25)$$

where

$$\theta = \cos^{-1}(|\sigma_1|/\sigma_\perp), \quad (26)$$

may range between 0 and  $\pi/2$ . The two dispersion relations yield four roots; assuming that  $k > 0$  we are interested in the two roots with positive real part. Setting

$$b = \frac{kv_A}{2\omega_c} \exp(\pm i\theta) \quad (27)$$

these two roots may be written

$$\omega_1 = \left( \sqrt{1 + b^2} + b \right) kv_A \quad (28)$$

and

$$\omega_2 = \frac{k^2 v_A^2}{\omega_1^*}, \quad (29)$$

where  $\omega_1^*$  is the complex conjugate of  $\omega_1$ . Note that  $|\omega_2| < kv_A < |\omega_1|$ .

The conductivity parallel to the field,  $\sigma_{\parallel}$  does not appear in the dispersion relation because  $\mathbf{E}'_{\parallel} = 0$  for these modes. The conductivity perpendicular to  $\mathbf{B}$ ,  $\sigma_{\perp}$ , determines  $\omega_c$  and sets the length scale at which the dispersion relation is modified from the ideal MHD case by the finite conductivity of the plasma, and the relative sizes of the Hall and Pedersen conductivities sets  $\theta$ .

Solving the linearised equations for the perturbations, we find:

$$\delta B_x = 0, \quad \delta B_y = \pm i \text{sign}(\sigma_1) \delta B_z. \quad (30)$$

$$\delta \mathbf{J} = \pm \text{sign}(\sigma_1) \frac{kc}{4\pi} \delta \mathbf{B}. \quad (31)$$

$$\frac{\delta \mathbf{v}}{v_A} = - \left( \frac{kv_A}{\omega} \right) \frac{\delta \mathbf{B}}{B} \quad (32)$$

$$\delta \mathbf{E}' = -i \text{sign}(\sigma_1) \exp(\pm i\theta) \frac{kv_A}{\omega_c} \frac{v_A}{c} \delta \mathbf{B}. \quad (33)$$

The perturbation to the electric field in the rest frame of the unperturbed fluid is

$$\delta \mathbf{E} = \mp i \text{sign}(\sigma_1) \left( \frac{\omega}{kv_A} \right) \frac{v_A}{c} \delta \mathbf{B}. \quad (34)$$

Equation (30) shows that the wave modes are circularly polarised, with the sense of polarisation depending on the sign of  $\sigma_1$ .

## 4.2 Wave propagation

The wave frequency  $\omega$  is plotted as a function of  $k$  in Fig. 8 for different choices of  $|\sigma_1|/|\sigma_2|$ . The solid curves give the real and imaginary parts of  $\omega$  for  $\sigma_1 = 0$ , the pure ambipolar diffusion case (see Kulsrud & Pearce 1969). For  $kv_A/\omega_c < 2$  the two circularly-polarised modes have the same frequency, thus one can construct linearly-polarised Alfvén waves. At low wave numbers, the modes reduce to Alfvén waves in the combined neutral and ionised fluid. As the wave number is increased the modes propagate at slightly below the Alfvén speed and are damped, the damping rate increasing as  $k^2$ . The phase speed drops significantly below the Alfvén speed at  $kv_A \approx \omega_c$ . At  $kv_A/\omega_c = 2$  the waves become evanescent, with two distinct modes.

The other curves plotted in Fig. 8 show how the modes are modified as the Hall conductivity is increased in importance. In general the damping rate is decreased because the Hall current is perpendicular to  $\mathbf{E}'$  and therefore does not contribute to the energy dissipation in the fluid. When the Hall conductivity is non-zero, the evanescent regime disappears.

The two circularly-polarised modes propagate with different phase speeds and damping rates because the Hall conductivity introduces a handedness into the fluid – the microphysical asymmetry between the positively- and negatively-

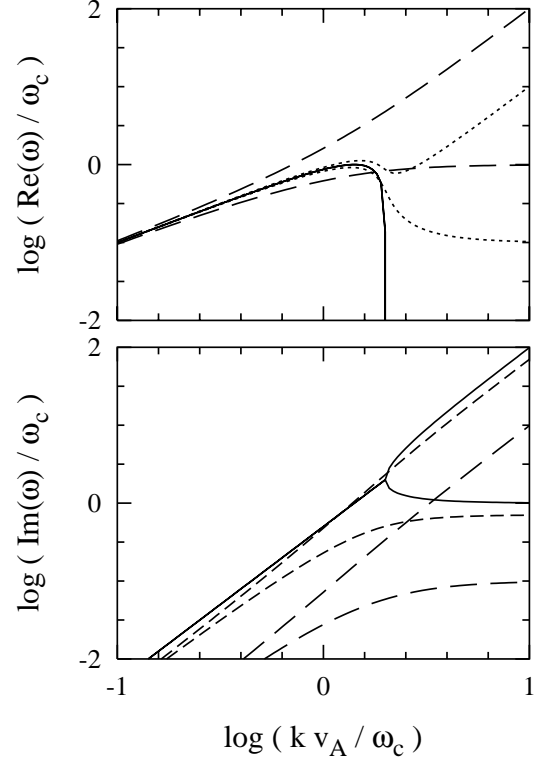


**Figure 8.** The dispersion relation for long-wavelength waves propagating parallel to the magnetic field in a uniform, weakly-ionised plasma. The real and imaginary parts of the wave frequency  $\omega$  (upper and lower panels respectively) are plotted as a function of (real) wave number,  $k$ . The characteristic frequency  $\omega_c$  is defined in eq. (23). The curves are distinguished by the ratio of the Hall and Pedersen conductivities,  $|\sigma_1|/|\sigma_2|$ : *solid* – 0; *dotted* – 0.1; *short-dashed* – 1; *long-dashed* – 10. For clarity, the curves for the real part of  $\omega$  for  $|\sigma_1|/|\sigma_2| = 1$ , and for the imaginary part for  $|\sigma_1|/|\sigma_2| = 0.1$  have been omitted as they are similar to those for  $|\sigma_1|/|\sigma_2| = 10$  and 0 respectively.

charged species is manifested as a dependence on the sign of the magnetic field, or the sense of circular polarisation.

For  $kv_A/\omega_c \gg 1$ , the roots of the dispersion relations with positive real part are

$$\frac{\omega_1}{\omega_c} \approx \left( \frac{kv_A}{\omega_c} \right)^2 \exp(i\theta) \quad (35)$$

and

$$\frac{\omega_2}{\omega_c} \approx \exp(i\theta) \quad (36)$$

A comparison of terms in the linearised induction equation yields

$$\left| \frac{\partial \mathbf{B} / \partial t}{\nabla \times (\mathbf{v} \times \mathbf{B})} \right| = \left| \frac{\omega}{kv_A} \right|^2. \quad (37)$$

For  $\omega_1$  or  $\omega_2$  this ratio is  $(kv_A/\omega_c)^2$  or  $(kv_A/\omega_c)^{-2}$  respectively. Thus  $\nabla \times \mathbf{E}'$  in the induction equation is balanced by  $\partial \mathbf{B} / \partial t$  and  $\nabla \times (\mathbf{v} \times \mathbf{B})$  respectively. Equation (32) shows that for these two modes, the ratio  $|\delta \mathbf{B} / B| / |\delta \mathbf{v} / v_A|$  is  $(kv_A/\omega_c)$  or  $(kv_A/\omega_c)^{-1}$ . The highly-damped mode  $\omega_1$  mode can be regarded as a wave in the *ionised* component fluid that is damped by collisions with the nearly static neutrals.

The  $\omega_2$  mode corresponds to transverse oscillations in the neutrals with small perturbations in the magnetic field and ionised component (c.f. Kulsrud & Pearce 1969). Note that both modes are undamped in the limit that  $\sigma_2 \rightarrow 0$ .

In the low-frequency limit  $kv_A/\omega_c \ll 1$ ,  $\omega_1$  and  $\omega_2$  become, to first order in  $kv_A/\omega_c$ ,

$$\frac{\omega}{kv_A} \approx 1 \pm \frac{kv_A}{2\omega_c} \cos \theta - i \frac{kv_A}{2\omega_c} \sin \theta \quad (38)$$

Thus the real part of  $\omega$  (i.e. phase speed) is hardly affected by  $\sigma$ , but the damping rate is dependent on both  $\sigma_1$  and  $\sigma_2$ . It should be noted that including the Hall term decreases the damping rate for a given  $k$  by increasing  $\omega_c$  and introducing a factor of  $\sin \theta$ . Thus the damping rate is reduced by a factor of  $\sin^2 \theta$  once  $\sigma_1$  is taken into account.

## 5 DISCUSSION

The evaluation of the conductivity tensor presented in §3 shows that for an MRN grain-size distribution the Hall conductivity is important for densities between  $10^7$  and  $10^{11} \text{ cm}^{-3}$ . PAHs, if present, reduce this range to  $10^9$ – $10^{10} \text{ cm}^{-3}$ . The magnitude of  $\sigma_1$  is sensitive to the slight difference (1% or less) in the number densities of positive and negative grains, and positive and negative PAHs, so a careful calculation of the ionisation balance at these densities is required to confirm these results. The sensitivity of the conductivity tensor to small changes in the relative abundances of these species potentially couples the qualitative dynamical behaviour of dense molecular gas to chemical reactions that affect the ionisation level in the gas, as these in turn may depend on the relative drift of the charged species and neutrals.

In dense molecular clouds the grain-size distribution is modified by the agglomeration of small grains through thermal collisions and the sweeping up of smaller particles by large particles (Ossenkopf 1993; Ossenkopf & Henning 1994). These processes remove most of the grains that have Hall parameters of order unity (grain sizes of order  $100 \text{ \AA}$ ), which tends to reduce the size of  $|\sigma_1|$ . In this case one expects the conductivity to resemble that for the 0.1 micron grain case (see Figs 1 and 2).

At a given density and magnetic field strength, the conductivity also depends on the assumed cosmic-ray ionisation rate per unit volume,  $\zeta n_H$ . There is a simple scaling law for  $\sigma$  as the fractional abundances  $n_j/n_H$  of the charged species depend only on the ratio  $n_H/\zeta$  (e.g. Nishi et al 1991). This allows  $\sigma$  to be written as a function of  $n_H/\zeta$  and  $B/\zeta$  rather than of  $n_H$ ,  $B$  and  $\zeta$  independently. Thus, for example, if  $\zeta$  is increased from our adopted value of  $10^{-17} \text{ H}^{-1} \text{ s}^{-1}$  to  $10^{-16} \text{ H}^{-1} \text{ s}^{-1}$ , the contours in Fig. 7 are shifted upwards and to the right by 1 logarithmic unit in each direction, significantly increasing the area covered by the  $|\sigma_1| = \sigma_2$  contour. The cosmic-ray flux is substantially reduced for densities in excess of  $10^{13} \text{ cm}^{-3}$ , which occur near the midplane in the inner few AU of protostellar disks, because the cosmic-ray flux is substantially reduced when the disk surface density exceeds the cosmic-ray attenuation column,  $96 \text{ g cm}^{-2}$ . In particular, the surface density at 1 AU from the Sun in the minimum solar nebula is approximately  $1200 \text{ g cm}^{-2}$  (Hayashi 1981). Under these conditions the charged particle

abundances are substantially reduced and the Hall contribution is negligible.

The Hall term introduces a definite handedness to the dynamical behaviour of the gas because of the differences in the properties of negatively- and positively-charged species. There is little change in dynamics on the largest scales, for which flux-freezing is a good approximation. On small length scales, the dynamical behaviour of the fluid is qualitatively altered, and is no longer unaffected under a global reversal of magnetic field direction. This has been previously noted in models for the acceleration of outflows from protostellar disks (Wardle & Königl 1993), where the relative orientation (i.e. parallel or anti-parallel) of the large-scale threading the disk and the angular velocity of the disk affects the ability of the field to centrifugally drive a disk wind. These effects are also apparent in models of C-type shock waves (Wardle 1997).

We chose to illustrate these effects by examining the consequences for Alfvén wave propagation, as the wave modes encapsulate the dynamical response of the fluid to perturbations. On large length scales, the Alfvén modes are damped more rapidly if the Hall contribution to  $\sigma$  is included, which could in principle have consequences for the survival of the Alfvén waves believed to support molecular clouds parallel to the magnetic field (Arons & Max 1975; Fatuzzo & Adams 1993; Gammie & Ostriker 1996), and for the contribution of wave dissipation to cloud heating (Zweibel & Josafatsson 1983). However at the relevant densities  $|\sigma_1| \ll \sigma_2$ , and in any case the factor of two difference that would obtain when  $|\sigma_1| \approx \sigma_2$  is of the same order as the theoretical and observational uncertainties in the field strength and charged particle abundances that determine the damping rate. Of more importance are the changes that occur on the length scales on which flux-freezing breaks down, when the two circularly-polarised Alfvén modes have different phase speeds and damping rates. For example, consider the following thought experiment that follows from the linear analysis of §4.1. Imagine at some initial time a homogeneous, static fluid permeated by a magnetic field of the form  $\mathbf{B} = B_0 \mathbf{x} + B_1 \sin kx \mathbf{y}$ , where  $B_0$  and  $B_1 \ll B_0$  are positive constants. How will the system evolve with time? In the ambipolar diffusion limit  $B_y$  will oscillate back and forth with nodes where  $\sin kx = 0$ , the oscillatory motion being damped by ambipolar diffusion. If the Hall term is important the motion is more complicated as one of the circular polarisations is more rapidly damped than the other. The field tends to twist back and forth, with an associated sloshing of the fluid. Thus the evolution is quite different in the two cases.

As the transport of angular momentum by magnetic fields and the breakdown of flux-freezing are believed to play important roles in the collapse of cloud cores to form stars (e.g. Shu, Adams & Lizano 1987; Mouschovias 1987), and the densities pass through the regime in which the Hall term is important, the consequences for the dynamics of collapsing cloud cores may be profound. Norman & Heyvaerts (1985) also noted that the Hall component of the conductivity tensor may become significant during star formation. However they dismiss its effects, claiming that the Hall current would rapidly lead to a slight charge separation, with the associated electric field quenching the Hall current. Although this can certainly occur for particular idealised ge-



ometries with well-defined boundaries, it is not clear that this mitigation of the Hall effect is generally true. For example, consider the quasistatic collapse of an axisymmetric cloud core through a magnetic field, and suppose that at some initial time the core is not rotating and the magnetic field is poloidal. Then the current is toroidal and the electric field in the neutral fluid frame is poloidal. Thus  $\nabla \times \mathbf{E}$ , hence  $\partial \mathbf{B} / \partial t$ , is poloidal, as is the Lorentz force  $\mathbf{J} \times \mathbf{B} / c$ . Thus the fluid velocities and the magnetic field remain poloidal as the system evolves. In contrast, if the Hall term is important, at  $t = 0$  the electric field has a poloidal component (as  $\mathbf{J}$  is still toroidal initially) and  $B_\phi$  will grow with time, forcing the fluid to also pick up a toroidal component. It is not hard to show that if the Hall and ambipolar diffusion components of the conductivity are of the same order that the toroidal components of the velocity and magnetic field will contribute significantly to the gravitational support of the core and therefore will significantly affect the dynamics of gravitational collapse. In this example the boundaries on which the charge is presumed to build up initially would have to be surfaces of constant azimuth, which cannot exist under the assumption of axisymmetry.

## 6 SUMMARY

In this paper we evaluated the conductivity tensor for weakly-ionised, dense molecular gas assuming a temperature of 30 K and a cosmic-ray ionisation rate of  $10^{-17} \text{ s}^{-1} \text{ H}^{-1}$ . We also considered the propagation of Alfvén waves in this medium. Our results are summarised as follows:

- (i) For single-size grains of size  $0.1 \mu\text{m}$ , the Hall term does not become significant.
- (ii) For an MRN grain-size distribution the Hall term becomes important between  $10^7$  and  $10^{11} \text{ cm}^{-3}$ .
- (iii) PAHs, if present, reduce this range to  $10^9$ – $10^{10} \text{ cm}^{-3}$ .
- (iv) The magnitude of the Hall conductivity is sensitive to the small differences in abundances of positive and negative grains, and positive and negative PAHs.
- (v) Long-wavelength Alfvén waves, for which flux freezing almost holds, are not much affected by the Hall term, apart from a reduced damping rate. Generally this reduction is not significant given the uncertainties in the parameters of the gas in molecular clouds.
- (vi) At wavelengths comparable to or less than the length scale on which flux-freezing breaks down, left- and right-circularly polarised Alfvén waves of the same frequency have distinct phase speeds and damping rates. For the typical case, the right-hand (left-hand) polarisation is most strongly damped for propagation parallel (anti-parallel) to the magnetic field. The other mode is damped on the ion-neutral coupling time scale, even at the shortest wavelengths.

We noted that the modification to Alfvén wave propagation is indicative of the change in the dynamical behaviour of the gas. In particular we suggested that the dynamics of the collapse of dense cloud cores may be profoundly affected.

We thank Leon Mestel for useful discussions. C. Ng was supported by an SRCfTA vacation scholarship. The Special Research Centre for Theoretical Astrophysics is funded by the Australian Research Council under the Special Research Centres programme.

## REFERENCES

- Arons, J. & Max, C. E. 1975, *ApJ*, 196, L77  
 Ciolek, G. E. & Mouschovias, T. C. 1993, *ApJ*, 418, 774  
 Cowling, T. G. 1957, *Magnetohydrodynamics* (New York: Interscience)  
 Cramer, N. F. & Vladimirov, S. V. 1997, *PASA*, 14, 170  
 Draine, B. T. 1980, *ApJ*, 241, 1021  
 Draine, B. T. & Lee, H. M. 1984, *ApJ*, 285, 89  
 Draine, B. T., Roberge, W. G. & Dalgarno, A. 1983, *ApJ*, 264, 485  
 Fatuzzo, M. & Adams, F. C. 1993, *ApJ*, 412, 146  
 Fiedler, R. A. & Mouschovias, T. C. 1993, *ApJ*, 415, 680  
 Gammie, C. F. & Ostriker, E. C. 1996, *ApJ*, 466, 814  
 Hayashi, C. 1981, *Prog Theor Phys Supp*, 70, 35  
 Kaufman, M. J. & Neufeld, D. A. 1996, *ApJ*, 456, 611  
 Kulsrud, R., Pearce, W. P. 1969, *ApJ*, 156, 445  
 Leger, A. & Puget, J. L. 1984, *AA*, 137, L5  
 Mathis, J. S., Rumpl, W. & Nordsieck, K. H. 1977, *ApJ*, 217, 425  
 Myers, P. C. & Goodman, A. A. 1988, *ApJ*, 326, L27  
 Nishi, R., Nakano, T. & Umebayashi, T. 1991, *ApJ*, 368, 181  
 Mouschovias, T. C. 1987, in *Physical Processes in Interstellar Clouds*, ed. G. E. Morfill and M. Scholer (Dordrecht: Reidel), 453  
 Nakano, T. & Umebayashi, T. 1986, *MNRAS*, 218, 663  
 Norman, C. & Heyvaerts, J. 1985, *AA*, 147, 247  
 Ossenkopf, V. 1993, *AA*, 280, 617  
 Ossenkopf, V. & Henning, T. 1994, *AA*, 291, 943  
 Parker, E. N. 1979, *Cosmical magnetic fields: their origin and their activity* (New York: Oxford University Press)  
 Pilipp, W., Hartquist, T. W., Havnes, O. & Morfill, G. E. 1987, *ApJ*, 314, 341  
 Shu, F., Adams, F. C. & Lizano, S. 1987, *ARA&A*, 25, 23  
 Spitzer, L. 1978, *Physical Processes in the Interstellar Medium* (New York: Wiley)  
 Umebayashi, T. & Nakano, T. 1990, *MNRAS*, 243, 103  
 Wardle, M. 1998, *MNRAS*, 298, 507  
 Wardle, M. & Draine, B. T. 1987, *ApJ*, 321, 321  
 Wardle, M. & Königl, A. 1993, *ApJ*, 410, 218  
 Zweibel, E. G. & Josafatsson, K. 1983, *ApJ*, 270, 511

This paper has been produced using the Royal Astronomical Society/Blackwell Science L<sup>A</sup>T<sub>E</sub>X style file.